Journal of Environmental Chemical Engineering 11 (2023) 110271

Contents lists available at ScienceDirect

Journal of Environmental Chemical Engineering

journal homepage: www.elsevier.com/locate/jece

Adsorption mechanism of As_2O_3 by Ca-Si-Al mineral: An experimental and DFT study

Guo-chang Song, Xing-yu Yang, Zhong-wei Li, Qiang Song [*,1,2]

Key Laboratory of Thermal Science and Power Engineering of Ministry of Education, Department of Energy and Power Engineering, Tsinghua University, Beijing 100084, China

ARTICLE INFO

Editor: Yunho Lee

Keywords:
Arsenic
Enhanced adsorption
Mineral
DFT
Mechanism

ABSTRACT

Arsenic (As) pollutants are highly toxic and using Ca-based minerals to adsorb As_2O_3 is effective for emission control. In this study, a fixed-bed experimental system was used to study the adsorption of As_2O_3 by the mixture of CaO, SiO_2, and Al_2O_3 at 1200 °C. The amount of As adsorbed by multiple minerals was higher than that by single minerals, indicating enhanced adsorption of As_2O_3 under the coupling effects of Ca, Si, and Al. The adsorption amount of As first increased and then decreased with an increase in the CaO:(SiO_2 +Al_2O_3) and SiO_2:Al_2O_3 ratios. Adsorbed As was mainly enriched in Ca-Si-Al mineral, including $Ca_2Al_2SiO_7$. Density Functional Theory calculation was conducted to study the As_2O_3 adsorption on the $Ca_2Al_2SiO_7$ (0 0 1) surface. The analysis of Mulliken charge and density of states showed that As_2O_3 molecules formed Al-O, O-As, and Ca-O bonds with the Al, O, and Ca sites. Si and Al in $Ca_2Al_2SiO_7$ enhanced the adsorption ability of Ca sites by promoting electron transfer. Si/Al ratio close to 1:1 is conducive to the formation of Si-O-Al structures, thus further enhancing the adsorption. The results can help optimize coal blending strategies and modify adsorbents to further reduce As emissions during coal combustion.

1. Introduction

Arsenic (As) pollutants in the atmosphere threat human health and ecological environment because of their high toxicity [1–4]. As is easily volatilized and discharged during coal combustion. Hence, coal combustion is an important emission source of As in the atmosphere [5]. The As emission from coal-fired devices have been restricted in some countries [6,7]. Although most of the As in the coarse particles can be removed by the dust collector and wet desulfurization device, part of As in the fine particles and the gas phase is emitted into the air [8–10]. Strengthening As retention in the solid phase facilitates the coordinated removal of As using air pollution control devices.

As is retained in both the coal combustion and post-combustion stages in a coal-fired system [11,12]. During the coal-combustion stage, As is partially retained in the solid products as residual As due to thermal stability or the retention by minerals in coal [13–15]. During the post-combustion stage, the cooling of the flue gas result in the transformation of As from gas phase to solid phase due to chemical reaction with the minerals in the ash or physical adsorption or condensation [16–19]. Strengthening the retention of As during coal combustion through coal blending or injection of mineral sorbents into the furnace can not only reduce As emission [20,21] but also help reduce the bioavailability and environmental risk of As in solid products [22,23]. Studying the effects of minerals on As at high temperatures is helpful for the development of the control technologies.

The mineral components in coal, namely Ca, Fe, Si and Al, are related to the retention of As. Seames et al. [24] found a strong correlation between As content and Ca and Fe in fly ash. Xu et al. [18] experimented on the As adsorption by ash and discovered that the As enrichment area on the fly ash surface mainly overlapped with Ca and Fe. These studies showed that Ca and Fe played key roles in As retention. The gaseous As in coal-fired systems is mainly in the form of As_2O_3 [25,26]. Several scholars have explored the mechanism of the reaction between mineral components and As_2O_3 at high temperatures. Yu et al. [27] compared the adsorption of As_2O_3 by CaO, Fe_2O_3, MgO, Al_2O_3, and SiO_2, and found that the adsorption capacity of CaO was significantly higher than that of other mineral oxides. Cao, Song, He, and Chen et al. [28–31] carried out the adsorption experiments of minerals on As_2O_3, and found

* Correspondence to: Department of Energy and Power Engineering, Tsinghua University, Haidian District, Beijing 100084, China.
E-mail address: qsong@tsinghua.edu.cn (Q. Song).
[1] ORCID: 0000-0002-5484-3594.
[2] Researcher ID: U-4938-2019.

https://doi.org/10.1016/j.jece.2023.110271
Received 29 March 2023; Received in revised form 20 May 2023; Accepted 1 June 2023
Available online 2 June 2023

that different forms of Ca-based minerals (CaO, $CaSiO_3$, and $CaSO_4$) can adsorb As_2O_3 and generate $Ca_3(AsO_4)_2$. In the coal combustion environment, the interaction of Si, Al, and Ca components in coal generates complex aluminosilicates [32], which might change the adsorption capacity and mechanism of As_2O_3 [33,34]. Song et al. [15] reported that the adsorption amount of As_2O_3 by mixture of CaO and kaolin was higher than the linear superposition of their individual adsorption capacities, indicating the strengthening of the adsorption ability by the co-effect of CaO and kaolin. Additionally, the resulting product exists in the form of a Ca-Si-Al-As complex salt rather than $Ca_3(AsO_4)_2$ [15]. Exploring the As_2O_3 adsorption mechanism under the joint action of Ca, Si, and Al minerals helps enhance As_2O_3 retention during coal combustion, which has not been reported yet.

Quantum chemical calculations based on the Density Functional Theory (DFT) can help understand the microscale mechanism of As_2O_3 adsorption. The adsorption mechanism of As_2O_3 by CaO and $CaSO_4$ has been discussed before. Yu and Fan et al. [26,35] studied the adsorption of As_2O_3 on CaO (0 0 1) surface and proposed that both Ca and O acted as adsorption sites. Li et al. [36] compared the adsorption of As_2O_3 on $CaSO_4$ with that on CaO and found that S could inhibit electron transfer from the O site to As, thus weakening the adsorption capacity. Yu et al. [27] found that As_2O_3 was adsorbed at the O sites on the SiO_2 (1 0 0) and Al_2O_3 (0 0 1) surface, while Xing et al. [37] discovered that As_2O_3 was adsorbed at the O and Al sites on the kaolin (0 0 1) surface. However, the adsorption energies of As_2O_3 on the SiO_2, Al_2O_3, and kaolin surfaces were significantly lower than those on the CaO surface, indicating that the adsorption is less stable [27,35,37]. Previous studies only focused on the adsorption of As_2O_3 by mineral oxides, including CaO, Al_2O_3, and SiO_2, but the microscale mechanism of As adsorption under the coupling action of these minerals remains unexplored.

In this study, co-combustion experiments of three mineral oxides (CaO, SiO_2 and Al_2O_3) and As model compounds were carried out at 1200 °C using a fixed-bed experimental system. The As adsorption amounts of different mineral components were obtained. The phase composition and micro-area composition of the adsorption product were analyzed to characterize As occurrence. DFT calculations were performed using the Cambridge Serial Total Energy Package (CASTEP) of Material Studio. The adsorption mechanism of As_2O_3 on the $Ca_2Al_2SiO_7$ (0 0 1) surface was revealed through adsorption energy calculations, charge transfer and partial density of states (PDOS) analysis. The enhanced As_2O_3 adsorption under the coupling action of Ca, Si, and Al was explored. The results can provide theoretical support for the development of As emission control technologies such as fuel blending [20] and adsorbent modification [38,39].

2. Experimental and calculational settings

2.1. Experimental settings

2.1.1. Materials

The minerals used in this study include CaO, SiO_2, and Al_2O_3 of analytical grade and were purchased from Shanghai McLean Biochemical Technology Co., Ltd. and p-aminophenylarsenic acid with a purity of 99 % was purchased from Shanghai Aladdin Biochemical Technology Co., Ltd. Cellulose was purchased from Sigma-Aldrich CO. LLC. with a purity of 99.8 %. The As model compound was prepared by mixing p-aminophenylarsenic acid with cellulose, which helps disperse p-aminophenylarsenic acid and ensure its uniform mixing with minerals. The As content of the model compound was 3.12 %. Before the experiments, the samples were dried at 105 °C for 10 h.

2.1.2. Experimental setup

Co-combustion experiments were conducted using a fixed-bed experimental system (Fig. 1). The structure of the system was described in a previous study [14]. The reaction gas consisted of N_2 and O_2, where the volume fraction of O_2 was 21 %. Prior to the experiment, the reactor was heated to 1200 °C and held for 30 min, and then the reaction gas was introduced from the top of the reactor until the atmosphere stabilized. A crucible with 0.3 g of sample was quickly inserted into the constant-temperature zone. After the set reaction time, the crucible was quickly removed, and solid products were collected for analysis.

2.1.3. Methods

Co-combustion experiments were carried out using 150 mg of minerals and 150 mg of As model compounds to study the adsorption of As_2O_3 by minerals. Our previous research [15] reported that the release ratios of As at 1200 °C were negatively correlated with the contents of Ca, Fe, Si, and Al in coal, which means that As was retained under the joint action of these mineral components. Therefore, the adsorption experiments were conducted at 1200 °C to reveal the mechanism. To compare the adsorption capacity of mineral oxides acting individually or

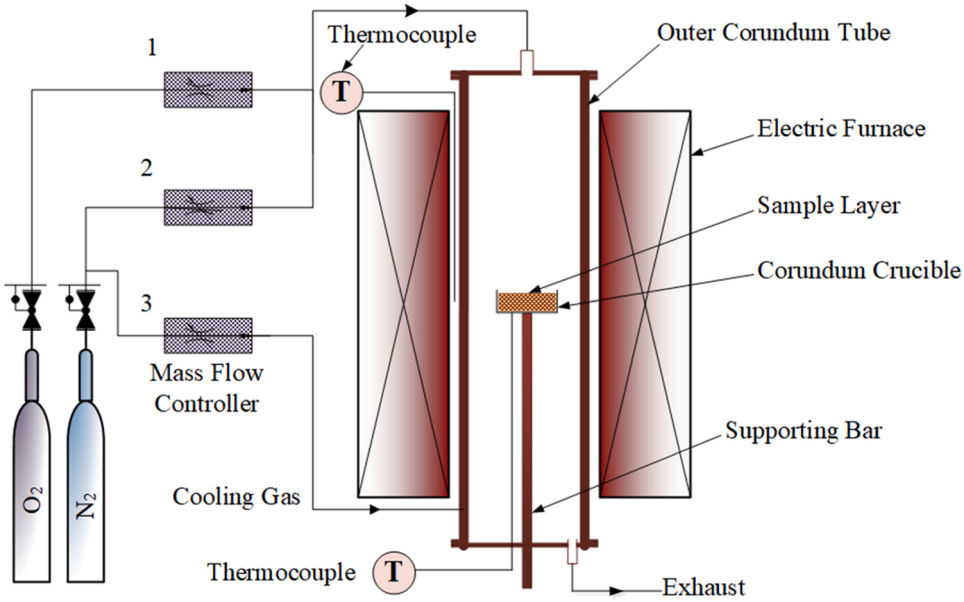

Fig. 1. Structure diagram of the fixed-bed experimental system [14].

jointly, the ratios of CaO, SiO_2, and Al_2O_3 were changed, while keeping the total mineral mass constant. Table 1 lists the mineral compositions used for different working conditions. The CO_2 in the outlet gas was detected using a Fourier transform infrared spectrometer (FTIR; Thermo Fisher Scientific Nicolet 6700, USA), and it was found that its concentration reached 0 after 10 min, which means that the sample was completely burned. The As in p-aminophenylarsenic acid will either be released or adsorbed by mineral components within 10 min

The As contents of the solid products were analyzed by first conducting digestion on the samples, which was described in a previous study [40]. An inductively coupled plasma emission spectrometer (ICP-OES; Leeman Labs Prodigy 7, USA) was used to analyze the As content. The sensitivity was 4.89×10^{-5} μg/mL. The analytical method was tested on the standard samples and the recovery rates of As were 99.1–100.2 %, which proved the accuracy of the method. The amount of As adsorbed by the minerals (mg/g) was calculated using Eq. (1).

$$R_{As} = \frac{m_{mi,p} \times C_{mi,p}}{m_{mi,r}} \quad (1)$$

where $m_{mi,r}$ is the mass (g) of the minerals before the reaction, $m_{mi,p}$ is the mass (g) of the solid products after the reaction, and $C_{mi,p}$ is the As content of the solid products (mg/g).

An X-ray diffraction (XRD; D8 Discover, Bruker, Germany) instrument was used to analyze the phase compositions of solid products. The 2θ range was set as 5–80° and the resolution was 0.02°. The microscale element distributions in the solid samples were analyzed by an electron probe microanalysis (EPMA; JXA8230, JEOL, Japan) system.

2.2. Calculational settings

DFT calculations were performed using the CASTEP program in Material Studio [41]. The Perdew-Burke-Ernzerhof (PBE) exchange and correlation functions of the Generalized Gradient Approximation (GGA) were chosen to describe the exchange and correlation interactions [42]. The electronic wave functions were expanded on a plane-wave basis [43] with a cut-off energy of 400.0 eV. The Broyden-Flechter-Goldfarb-Shanno (BFGS) method was used for geometry optimization [44] and the convergence criteria were as follows: (1) self-consistent field (SCF) $< 1.0 \times 10^6$ eV/atom; (2) energy $< 1.0 \times 10^5$ eV/atom; (3) displacement < 0.001 Å; (4) force < 0.03 eV/Å; (5) stress < 0.05 Gpa.

In this study, $Ca_2Al_2SiO_7$ was used as a typical calcium aluminosilicate mineral to investigate the adsorption of As_2O_3. Cell parameters were obtained from Swainson et al. [45]. Considering the Si-Al disorder in aluminosilicate, the Si-Al order, which ensured the lowest energy of the system according to Thayaparam et al. [46], was adopted to build the cell and slab models. The optimized cell parameters are listed in Table S1, and the relative deviation from the results of Swainson et al. [45] was within 1 %, which proved the reliability of the calculation method. The (0 0 1) surface was reported as the dominant crystal plane of $Ca_2Al_2SiO_7$ [47]; therefore, it was used to study the adsorption of As_2O_3. A series of *m*-layer slab models with $n \times n$ horizontal planes were established to compare the adsorption energies. The superficial layer of atoms was relaxed, whereas the remaining layers were fixed. The vacuum region between the slabs was set at 15 Å. The energy of optimized slabs when calculating with different cut-off energies and *k*-points are shown in Tables S2 and S3. It can be seen that when the cut-off energy was 400 eV or higher, the change in energy was within 0.01 eV/atom, which means that the accuracy was sufficient. A *k*-point mesh of $2 \times 1 \times 1$ was chosen for the calculations. The adsorption energy E_{ad} (kJ/mol) was calculated using Eq. (2):

$$E_{ad} = E_{product} - E_{adsorbent} - E_{adsorbate} \quad (2)$$

where $E_{product}$, $E_{adsorbent}$, and $E_{adsorbate}$ are the energies (kJ/mol) of the adsorption product, adsorbent, and adsorbate, respectively.

As shown in Table S4, the E_{ad} obtained by the two-layer slab model with a 2×2 horizontal plane was − 237.19 kJ/mol, and the relative deviation from those obtained by the larger slab models was within 1 %. To improve the calculation efficiency, a two-layer slab model with a 2×2 horizontal plane was used for further calculations (Fig. 2).

The As_2O_3 molecule was placed in a $20 \times 20 \times 20$ Å^3 periodic box, and geometry optimization was conducted. A *k*-point mesh of $1 \times 1 \times 1$ was chosen, and the cutoff energy was 380.0 eV [35]. The As_2O_3 molecule may be presented as a chain-type, horn-type, or trigonal bipyramid-type. The most stable structure of As_2O_3 is the chain type at temperatures above 1173 °C [48], which was adopted in this study. The calculated bond lengths and angles of the As_2O_3 molecules are shown in Table S5.

Table 1
Mass of minerals in the co-combustion experiments (mg).

Sample	CaO	SiO_2	Al_2O_3
1	150	0	0
2	0	150	0
3	0	0	150
4	50	100	0
5	50	0	100
6	0	75	75
7	50	75	25
8	50	67	33
9	50	50	50
10	50	33	67
11	50	25	75
12	30	60	60
13	70	40	40
14	100	25	25

3. Results and discussion

3.1. Experimental study of As_2O_3 adsorption by composite minerals of CaO, SiO_2, and Al_2O_3

The adsorption amounts of As when CaO, SiO_2, and Al_2O_3 acted alone or together after the mineral and As model compounds were burned at 1200 °C for 10 min are shown in Table 2. The amounts of adsorbed As in CaO, SiO_2, and Al_2O_3 were 3.0, 0, and 0.2 mg/g, respectively. When CaO was blended with SiO_2 in a mass ratio of 1:2, the adsorption amount of As reached 2.0 mg/g, which was higher than the linear superposition of As adsorption amount when each mineral acted individually (1.0 mg/g). This indicates that As adsorption was enhanced

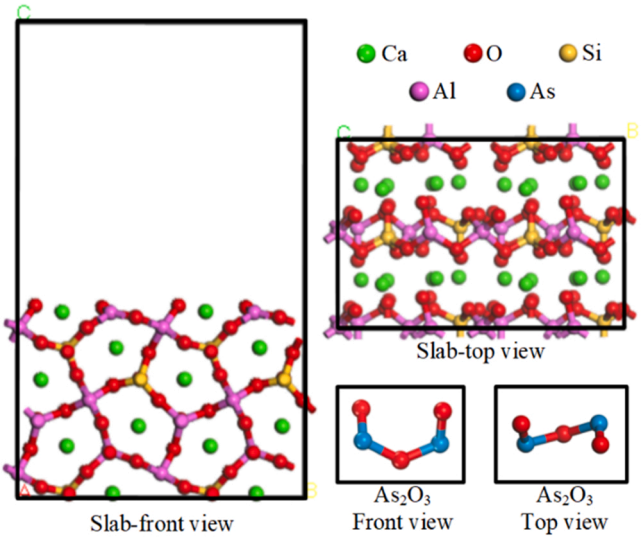

Fig. 2. Structures of $Ca_2Al_2SiO_7$ slab model and As_2O_3 molecule.

Table 2
Adsorption amount of As by single mineral/multi-minerals (mg/g).

Minerals	Adsorption amount of As
150 mg CaO	3.0
150 mg SiO_2	0
50 mg CaO + 100 mg SiO_2	2.0
150 mg Al_2O_3	0.2
50 mg CaO + 100 mg Al_2O_3	1.5
75 mg SiO_2 + 75 mg Al_2O_3	0.2

by the coupling of SiO_2 and CaO. A similar phenomenon was observed between Al_2O_3 and CaO.

The adsorption capacity of As was further improved when CaO, SiO_2, and Al_2O_3 were blended. The mass of CaO in the mineral was maintained at 50 mg, and the total mass of SiO_2 +Al_2O_3 was 100 mg. The ratio of SiO_2:Al_2O_3 varied, and the adsorption amounts of As are shown in Fig. 3. With the decrease of the SiO_2:Al_2O_3 ratio, the adsorption amount of As first increased and then decreased, reaching the maximum value of 3.8 mg/g when SiO_2:Al_2O_3 = 1:1. This indicates a coupling effect between Si and Al, which can further enhance the adsorption of As by Ca-Si-Al minerals. The coupling effect was stronger when the ratio of the two was 1:1.

Fig. 4 shows the change in As adsorption amount as the mass ratio of CaO: (SiO_2 +Al_2O_3) was adjusted while keeping the SiO_2:Al_2O_3 ratio constant at 1:1. Adding 1/3 mass fraction of SiO_2 +Al_2O_3 to CaO led to a significant increase in As adsorption. However, the adsorption amount of As gradually decreased with the increasing ratio of SiO_2 +Al_2O_3 because of the decrease in the effective component Ca. When only Si and Al were present in the minerals, the As adsorption amount was less than 0.2 mg/g.

The effect of the Si-to-Al ratio on As adsorption is related to the morphological changes of Ca-based minerals. Fig. 5 shows the XRD patterns of the solid products obtained when CaO:(SiO_2 +Al_2O_3)= 1:2 and SiO_2:Al_2O_3 were 1:0, 1:1, and 0:1. When SiO_2: Al_2O_3 = 1:0, CaO reacts with SiO_2 to produce Ca_2SiO_4 with some unreacted CaO and SiO_2. When SiO_2: Al_2O_3 = 0:1, CaO reacted with Al_2O_3 to produce $CaAl_4O_7$ and $Ca_{12}Al_{14}O_{33}$. Cao et al. [28] found that $CaSiO_3$ had a stronger adsorption capacity for As_2O_3 than CaO. He et al. [29] found that the CaO–$Ca_{12}Al_{14}O_{33}$ system had a stronger adsorption capacity for As than CaO. Therefore, the coupling of Si and Al with Ca enhanced the As adsorption owing to the formation of calcium silicate and calcium aluminate. When Si and Al were present simultaneously, the product contained $Ca_2Al_2SiO_7$ in addition to Ca_2SiO_4, $CaAl_4O_7$, and $Ca_{12}Al_{14}O_{33}$.

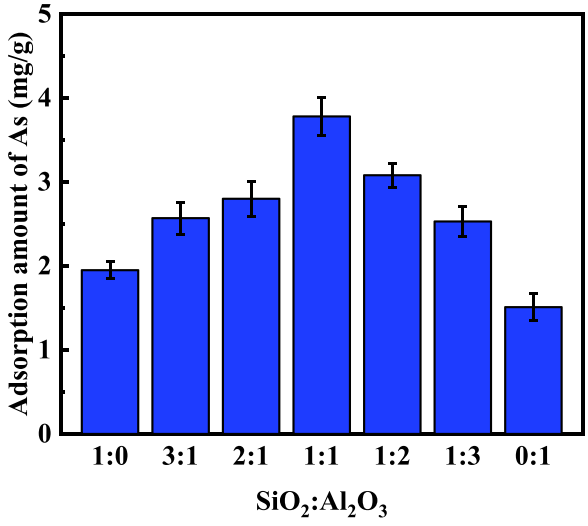

Fig. 3. Adsorption amount of As by Ca-Si-Al minerals with different SiO_2: Al_2O_3 ratios.

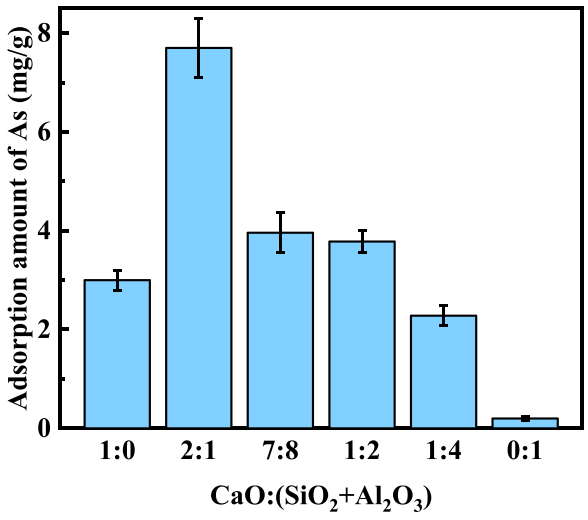

Fig. 4. Effects of CaO:(SiO_2 +Al_2O_3) ratio on the adsorption amount of As.

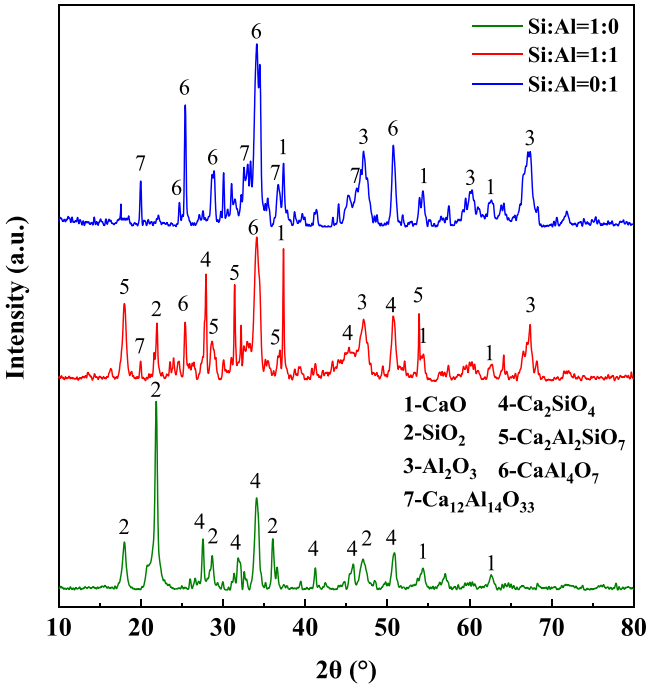

Fig. 5. XRD patterns of adsorption products with Si:Al= 1:0, 1:1, and 0:1.

Therefore, the coupling effect of Si and Al further strengthened the adsorption of As by Ca-containing minerals, which might be attributed to the formation of calcium aluminosilicate.

Fig. 6 shows the results of the micro-area composition analysis of the adsorption products when CaO: (SiO_2 +Al_2O_3)= 1:2 and SiO_2: Al_2O_3 = 1:1. It can be seen that the As enrichment region had both Si and Al enrichment (region 1), whereas the As content in the region with only Si or Al enrichment was significantly lower (regions 2 and 3). The XRD characterization results suggest that As was enriched in Ca-Si-Al minerals (such as $Ca_2Al_2SiO_7$). The adsorption capacity of Ca aluminosilicate on As_2O_3 was stronger than that of calcium silicate and calcium aluminate. Therefore, in the system of CaO+SiO_2 +Al_2O_3, when SiO_2: Al_2O_3 = 1:1, it is most advantageous to convert CaO into calcium aluminosilicate to achieve the largest adsorption amount of As.

The components of Si and Al can strengthen the adsorption capacity of Ca-based minerals to As and have a coupling effect between them. The

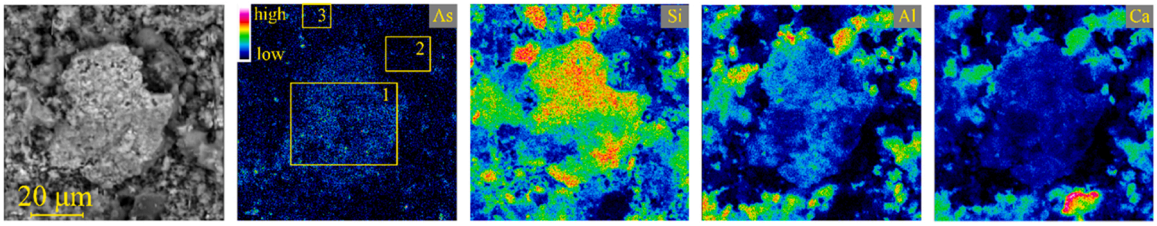

Fig. 6. Elemental mapping of adsorption products with Si:Al= 1:1.

results of the phase composition and micro-area composition analysis of the product show that the existence of this coupling effect is because of the formation of Ca-Si-Al minerals (such as $Ca_2Al_2SiO_7$). These minerals have a stronger adsorption capacity for As_2O_3 than calcium silicate and calcium aluminate. Therefore, the adsorption mechanism of $Ca_2Al_2SiO_7$, which was a typical Ca-Si-Al mineral, to As_2O_3 was analyzed by DFT calculation in Section 3.2.

3.2. DFT study of As_2O_3 adsorption on $Ca_2Al_2SiO_7$ surface

Fifty-six adsorption structures of As_2O_3 molecules on the $Ca_2Al_2SiO_7$ (0 0 1) surface were obtained after structure optimization, and the adsorption energy ranged from − 557.29 kJ/mol to − 135.14 kJ/mol. The maximum adsorption energy of $Ca_2Al_2SiO_7$ to As_2O_3 reached − 557.29 kJ/mol, which was significantly higher than the reported adsorption energy of CaO, SiO_2, Al_2O_3, and kaolin to As_2O_3 (−391.40, −156.40, −203.23, and −385.00 kJ/mol, respectively) [25,35,37]. This indicates that $Ca_2Al_2SiO_7$ had a stronger adsorption capacity for As_2O_3.

According to the order of the adsorption energy from high to low, the adsorption structures were numbered G1–56. The top and side views of each adsorption structure are listed in Table S6. The active adsorption sites on $Ca_2Al_2SiO_7$ (0 0 1) surface include unsaturated Al, nonbridging O, and Ca sites. The O atom in the As_2O_3 molecule was usually located at an unsaturated Al or Ca site, whereas the As atom was usually located at a nonbridging O site. The structure G1 with the highest adsorption energy was taken as an example to analyze the adsorption mechanism of As_2O_3 on the $Ca_2Al_2SiO_7$ (0 0 1) surface.

Fig. 7 shows the structural diagram of G1. As(1), As(2), O(1), O(2), and O(3) originally belonged to the adsorbate As_2O_3 molecule. Compared with Fig. 2, it can be seen that As_2O_3 molecules underwent deformation after adsorption, and the distance between As(1) and O(2) increased from 1.808 Å to 3.564 Å. The As(1)-O(1), As(2)-O(2), and As (2)-O(3) distances were 1.794, 1.711, and 1.650 Å, respectively. The changes were minimal when compared with the bond lengths of 1.621, 1.805, and 1.623 Å of the As_2O_3 molecules before adsorption. O(1) and O(2) were located at the unsaturated Al(1) and Al(2) sites on the surface at distances of 1.802 and 1.783 Å, respectively, which were close to the

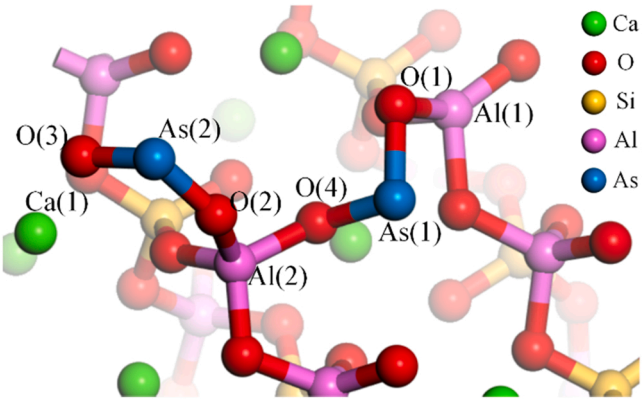

Fig. 7. Structure of G1 with the highest E_{ad} of − 557.29 kJ/mol.

length of the Al-O bond. As(1) was located at the surface nonbridging O (4) site at a distance of 1.784 Å. O(3) was located at the surface Ca site at a distance of 2.324 Å. The surface structure of $Ca_2Al_2SiO_7$ (0 0 1) also changed: the length of the Al(2)-O(4) bond changed from 1.664 Å to 1.813 Å, and the position of Al(2) shifted towards the O(2) atom in the As_2O_3 molecule. The change in the structural parameters indicates that the interaction between As_2O_3 molecules and surface atoms was strong, which might be accompanied by the transfer of valence electrons and the formation of chemical bonds.

Table 3 shows the distribution of the Mulliken charges before and after adsorption. A negative value of $\triangle q$ indicates that the atom lost electrons, and a positive value indicates that the atom gained electrons. The $\triangle q$ values of As(1), As(2), O(1), O(2), and O(3) were added, and the As_2O_3 molecule gained 0.36 e from the surface of the adsorbent. A significant electron transfer occurred at each adsorption site. O(3) received electrons from Ca(1) and O(2) received electrons from Al(2). O(1) obtained electrons from Al(1), As(1), and O(4). After adsorption, the Mulliken charges of O(1), O(2), and O(4) were similar, indicating that the chemical environment was similar; that is, the As and Al atoms were connected with bridge O. Electron transfer means that As_2O_3 molecules formed bonds with the surface atoms of the adsorbent, including O-Al, As-O, and O-Ca bonds.

The bonding mechanism can be analyzed using PDOS. Fig. 8(a) shows the density of states (DOS) of the s and p orbitals before and after adsorption of the O(1) atom in the As_2O_3 molecule. It can be seen that the PDOS peak of the s orbital shifted to the lower energy levels (from −9.3 eV to −10.3 eV, from −17.4 eV to −18.3 eV, from −18.6 eV to −20.0 eV), which indicates that the atomic energy decreased. However, the s orbitals did not participate in bonding, so there was no splitting of the peak of PDOS. The p-orbital electrons also transferred to the lower energy level, and the energy level splitting occurred in the range of − 7.3 eV to − 3.7 eV, which indicates that the O(1) atom and the adsorbent surface atom formed a new chemical bond. Fig. 8(b) shows the DOS of the s and p orbitals before and after the adsorption of the Al (1) atoms on the adsorbent surface. After adsorption, the p-orbital electrons transferred to the high-energy range as a whole, and the peak in the range of 2.1–5.7 eV decreased significantly, which means that Al (1) atoms lost electrons. According to the Mulliken charge analysis results, these electrons were transferred to the O(1) atom. Comparing the PDOS of O(1) and Al(1) atoms, there were energy level overlapped at − 5.6 eV, − 5.0 eV, 4.4 eV, 3.1 eV, 4.0 eV, and 4.4 eV, which indicates that the electronic orbitals were hybridized and O-Al bond was formed.

Fig. 8(c) and (d) show the PDOS diagrams of the As(1) atom in the As_2O_3 molecule and O(4) atom on the surface of the adsorbent, respectively. The electrons of s and p orbital of As(1) atom were transferred to the low energy level. The p orbital electrons splitted in the range of − 7.3 eV to − 1.1 eV and 4.5–7.6 eV, indicating that they participated in the formation of new chemical bonds. The electrons of O (4) atom also transferred to the lower energy level, and energy level splitting occurred in the range of − 7.3 eV to − 1.3 eV. The PDOS peak of the As(1) and O(4) atoms decreased after adsorption, which indicates that electrons were lost during adsorption, which was consistent with the results of the Mulliken charge analysis. There were energy level overlaps between the two at − 6.4 eV, − 5.7 eV, - 3.9 eV, and 2.1 eV, indicating the formation of an As-O covalent bond.

Table 3
Mulliken charge (q) of atoms before/after adsorption and the charge transfer (e).

Atom	As (1)	As (2)	O (1)	O (2)	O (3)	O (4)	Al (1)	Al (2)	Ca (1)
q_{before}	1.26	1.26	-0.80	-0.92	-0.80	-1.14	1.70	1.73	1.28
q_{after}	1.28	1.29	-1.03	-1.02	-0.88	-1.04	1.74	1.82	1.36
$\triangle q$	-0.02	-0.03	+0.23	+0.10	+0.08	-0.10	-0.04	-0.09	-0.08

Fig. 8(e) and (f) show the PDOS diagram of the O(2) atom in the As_2O_3 molecule and the Al(2) atom on the surface of the adsorbent, respectively. The electrons of the O(2) atom transferred significantly to the lower energy level, and energy level splitting occurred in the range of − 7.1 eV to − 1.1 eV. Similar phenomena also existed in the electrons of the Al(2) atom, and resonance occurred with the p-orbital electrons of the O(2) atom at − 9.9 eV, − 5.9 eV, − 4.5 eV, − 2.7 eV, and 4.5 eV levels. This indicates the formation of an O-Al covalent bond.

Fig. 8(g) and (h) show the PDOS diagram of the O(3) atom in the As_2O_3 molecule and the Ca(1) atom on the surface of the adsorbent, respectively. The electrons of the O(3) atom were transferred to a lower energy level. The energy level of the electron of the Ca(1) atom did not change significantly after adsorption, but the peak of DOS of the p-orbital electron in the range of 2.1–5.7 eV decreased, indicating that Ca (1) lost electrons. No energy-level splitting or resonance was observed for O(3) and Ca(1), confirming the formation of ionic bonds.

3.3. Mechanism analysis on the enhanced adsorption of As_2O_3 by Ca, Si, and Al

By comparing the adsorption of As_2O_3 at similar sites on the surfaces of $Ca_2Al_2SiO_7$, CaO, SiO_2, and Al_2O_3, the mechanism of enhanced adsorption under the coupling of Ca, Si, and Al was revealed.

The adsorption of As_2O_3 by CaO and $Ca_2Al_2SiO_7$ was compared, and the influence of Si and Al on the adsorption ability of Ca sites was analyzed. In the adsorption structure of CaO to As_2O_3, the Ca-O bond length was 2.587 Å, and the bond population was 0.15 [35]. The Ca-O bond length formed by the As_2O_3 adsorption on the surface of $Ca_2Al_2SiO_7$ was shorter (2.327 Å) when compared with that of CaO, confirming that the bonding was stronger. Fig. 9 shows the DOS of the Ca-O bond in As_2O_3 adsorbed by CaO and $Ca_2Al_2SiO_7$. Compared with the CaO adsorption structure, the Ca-O bonding molecular orbital in the $Ca_2Al_2SiO_7$ adsorption structure moved to the lower energy level, and the anti-bonding molecular orbital moved to the higher energy level, resulting in a wider energy band and indicating a more stable bonding. The results suggest that the presence of Si/Al enhanced the adsorption ability of the Ca sites.

Ca in $Ca_2Al_2SiO_7$ had a higher reactivity than that in CaO. In CaO, the distance between Ca and the surrounding O atoms was 2.418 Å, and the Mulliken charge of Ca was 1.12 e. In $Ca_2Al_2SiO_7$, the distance between Ca and O atoms was 2.073 Å, and the Mulliken charge of Ca was 1.28 e; Ca had higher positive electricity in $Ca_2Al_2SiO_7$, so it had a stronger attraction to O in As_2O_3 molecules. Fig. 10 shows the DOS analysis results for CaO and $Ca_2Al_2SiO_7$ before adsorption. The existence of Si/Al reduced the energy gap of the Ca atom from 5.3 eV to 3.3 eV, which made the outer electrons of Ca more prone to transition, so it was easier to react with O.

Ca did not enhance the adsorption of As_2O_3 at the Si and Al sites. The length of the Al-O bond in the $Ca_2Al_2SiO_7$ adsorption structure was similar to that of the Al_2O_3 adsorption structure, which were 1.795 and 1.802 Å, respectively, indicating similar bonding strength [27]. Compared with the As_2O_3 structure adsorbed by SiO_2, the Si-O bond in the $Ca_2Al_2SiO_7$ adsorption structure was longer, and the bond population was lower, indicating weaker bonding [27]. The length of the As-O bond in the $Ca_2Al_2SiO_7$ adsorption structure was similar to those of the CaO and Al_2O_3 adsorption structures, which were 1.783, 1.791 and 1.785 Å, respectively, indicating that the difference in the adsorption of O sites was not significant. Therefore, the coupling of Ca, Si, and Al enhanced the adsorption of As, mainly because Si/Al enhanced the adsorption ability of the Ca site.

The experimental results in Section 3.1 show that Si and Al both strengthened the adsorption capacity of Ca to As, and there was a coupling effect between Si and Al that further strengthened the adsorption of As, especially when the ratio of the two was close to 1:1. This effect is related to the order of Si and Al in the lattice structure of calcium aluminosilicate [49]. In $Ca_2Al_2SiO_7$, Si or Al was connected with other Si or Al through bridge O, forming Si-O-Si, Si-O-Al, or Al-O-Al sturctures. The adsorption would be affected when the chemical environment of the adsorption sites changed [50,51]. Fig. 11(a) shows the original adsorption structure (G1), where the adsorption site, Al, was connected to the neighboring Al and Si through Al-O-Al and Al-O-Si sturctures. Fig. 11(b) shows the adsorption structure (Sub1) obtained by replacing the adjacent Si (Si(5) and Si(6)) of the adsorption site with Al (Al(5) and Al(6)) based on G1, where the adsorption site (Al) was connected with the other two Al atoms through the Al-O-Al sturctures. Fig. 11(c) shows the adsorption structure (Sub2) obtained by replacing the adjacent Al (Al(3) and Al(4)) of the adsorption site with Si (Si(3) and Si(4)), where the Al adsorption site was connected to the other two Si atoms through the Al-O-Si sturctures.

The comparison in Fig. 11 shows that the adsorption sites of As_2O_3 remained unchanged after the Si/Al rearrangement, but the adsorption energy and adsorption structural parameters changed significantly (Table 4). After replacing the Si adjacent to the G1 adsorption site with Al and forming the Al-O-Al sturctures (Sub1), the adsorption strength of As_2O_3 decreased, and the adsorption energy decreased slightly to − 549.99 kJ/mol. The analysis of the bonding strength and electron transfer reveals the reason for the decrease in the adsorption strength. The bond length of O(2)-Al(2) increased from 1.784 to 1.792 Å, indicating that the O(2) atom in the As_2O_3 molecule was further away from the adsorbent surface. The bond population decreased from 0.36 to 0.33, confirming weaker bonding because of the less overlapping of O-Al electron clouds. The Mulliken charge of Al(2) decreased from 1.82 e to 1.79 e, which can be attributed to the decrease in the number of electron transfers. The changes of bond length and population between As(1) and O(4) were similar to those between O(2) and Al(2), whereas the bond length and bond population of O(1)-Al(1) and O(3)-Ca(1) were almost unchanged. This shows that the adsorption of the Al(2) and O(4) sites in Sub1 was weaker than that of the G1 structure. However, after replacing Al with Si and forming Al-O-Si sturctures on both sides (Sub2), the adsorption of As_2O_3 was significantly enhanced, and the adsorption energy was increased to − 615.57 kJ/mol. The bond lengths of the O(1)-Al(1), As(1)-O(4), and O(3)-Ca(1) bonds decreased by 0.020, 0.039, and 0.039 Å, respectively, and the population increased by 0.01, 0.07, and 0.03, respectively, indicating stronger bonds. The Mulliken charge of the As_2O_3 molecule was − 0.99 e, which was lower than that of the G1 structure (−0.36 e), indicating that As_2O_3 molecules in the Sub2 structure gained more electrons from the adsorbent. Moreover, the Mulliken charge of Al(1) and Al(2) also increased. This shows that the adsorption of Al(1), Al(2), and Ca(1) sites in the Sub2 structure were strengthened compared with the G1 structure. The formation of Si-O-Al structure promoted the adsorption of As_2O_3 on the surface of $Ca_2Al_2SiO_7$.

In summary, the coupling mechanism of enhanced As_2O_3 adsorption by Ca, Si, and Al was clarified. The Ca-O(As_2O_3) bond in the $Ca_2Al_2SiO_7$ structure was more stable compared with CaO, as Si and Al promoted the transfer of electrons from the outer layer of Ca to As_2O_3, thereby strengthening the adsorption capacity of the Ca site. Ca had no

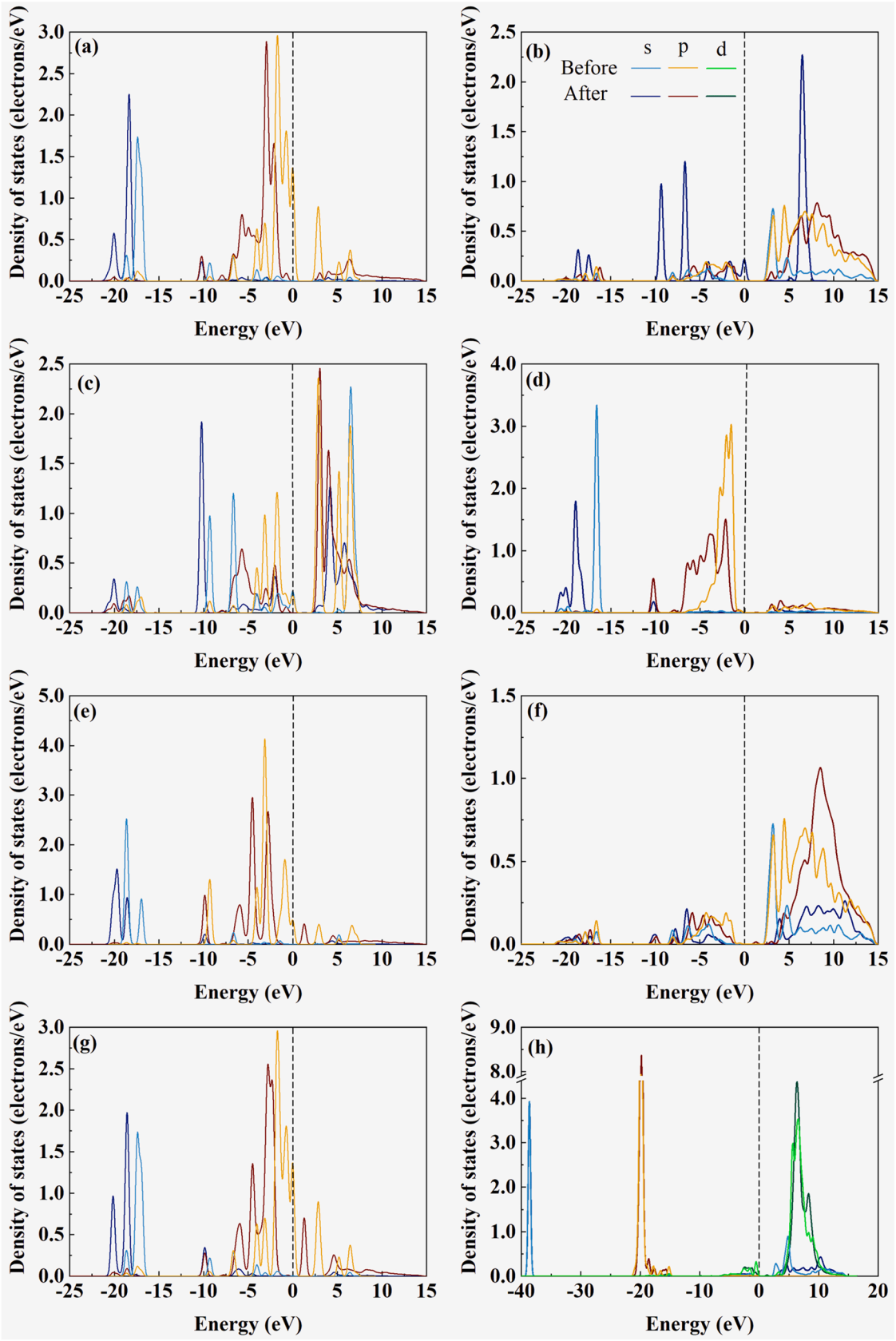

Fig. 8. PDOS of As_2O_3 adsorption on $Ca_2Al_2SiO_7$ surface: (a) O(1); (b) Al(1); (c) As(1); (d) O(4); (e) O(2); (f) Al(2); (g) O(3); (h) Ca(1).

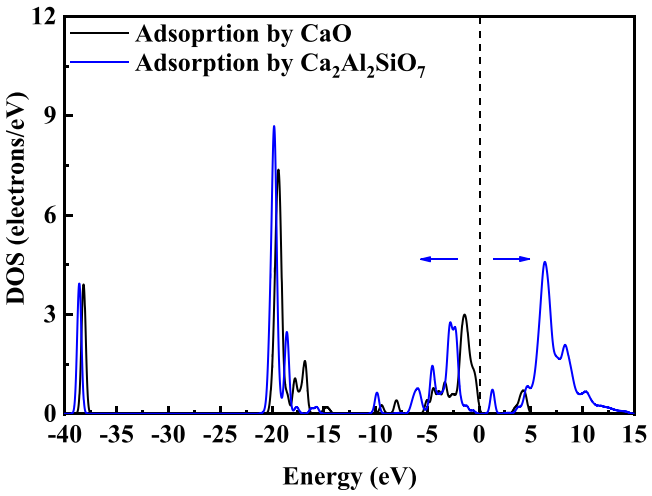

Fig. 9. LDOS of Ca-O bond in adsorption structure of CaO and $Ca_2Al_2SiO_7$.

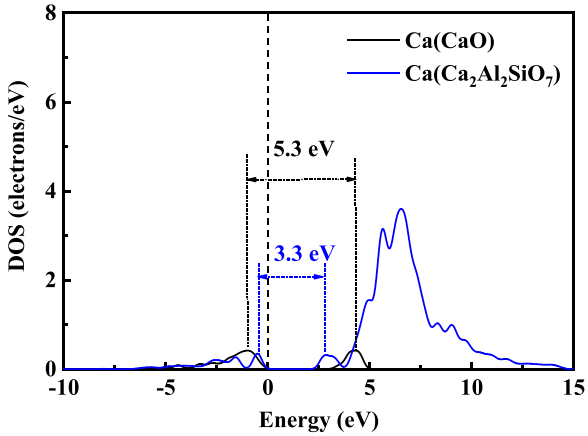

Fig. 10. DOS of Ca in CaO and $Ca_2Al_2SiO_7$ before adsorption.

strengthening effect on the adsorption of Si and Al sites. The order of Si/Al had a significant influence on the adsorption of As. The bond lengths of the Al-O(As_2O_3) and Ca-O(As_2O_3) bonds were shorter when the Al site was connected to Si on both side, which means that the bonding was more stable and therefore the adsorption energy was higher. This explains why the coupling effect of Si and Al strengthened the adsorption of As_2O_3 in Section 3.1. The closer the Si/Al ratio was to 1:1, the more conducive it was to the formation of Si-O-Al sturctures in minerals, resulting in the stronger adsorption capacity of As_2O_3.

4. Conclusions

The As adsorption characteristics were investigated for the mixture of CaO, SiO_2, and Al_2O_3 at 1200 °C. Adding SiO_2 +Al_2O_3 to CaO significantly enhanced the adsorption of As. The As adsorption amount first increased and then decreased with an increase in the SiO_2:Al_2O_3 ratio, reaching a maximum value when SiO_2:Al_2O_3 = 1:1. With the mass fraction of SiO_2 +Al_2O_3 increasing and CaO decreasing, the As adsorption amount was gradually decreased. The coupling effect of Si and Al strengthened the adsorption of Ca-based minerals to As. The adsorbed As was enriched in the Ca-Si-Al minerals (such as $Ca_2Al_2SiO_7$).

The adsorption mechanism of As_2O_3 on the (0 0 1) surface of $Ca_2Al_2SiO_7$, a typical Ca-Si-Al mineral, was investigated. There were 56 adsorption structures of As_2O_3 on the surface of $Ca_2Al_2SiO_7$, and the adsorption energy was between − 557.29 kJ/mol and − 135.14 kJ/mol. The active adsorption sites included unsaturated Al, nonbridging O, and Ca sites. The O atom in the As_2O_3 molecule was located at the unsaturated Al or Ca sites to form Al-O and Ca-O bonds, whereas the As atom was located at the nonbridging O site to form an As-O covalent bond.

The strengthening mechanism under the coupling of Ca, Si, and Al on the adsorption of As_2O_3 was revealed. Si/Al facilitated the transfer of electrons from Ca to As_2O_3 molecules, thereby enhancing the adsorption capacity of Ca site. Ca had no strengthening effect on the adsorption of As_2O_3 at Si and Al sites. The order of Si/Al on the surface of $Ca_2Al_2SiO_7$ significantly affected the adsorption of As. The formation of Si-O-Al sturctures promoted the adsorption of As_2O_3 at the Ca and Al sites.

These results provide theoretical support for As emission control by strengthening As adsorption at high temperatures, which is conducive to the collaborative removal of particulate As by pollution control device. It is recommended that blending coals with difference in the contents of Ca, Si, and Al will promote the As adsorption under the coupling of these

Table 4
E_{ad}, bond length, and bond population of structures G1, Sub1, and Sub2.

Structure		G1	Sub1	Sub2
E_{ad} (kJ/mol)		-557.29	-549.99	-615.57
Bond length (Å)	O(1)-Al(1)	1.802	1.802	1.782
	O(2)-Al(2)	1.784	1.792	1.832
	As(1)-O(4)	1.783	1.794	1.744
	O(3)-Ca(1)	2.324	2.323	2.285
Bond population	O(1)-Al(1)	0.37	0.37	0.38
	O(2)-Al(2)	0.36	0.33	0.28
	As(1)-O(4)	0.36	0.34	0.43
	O(3)-Ca(1)	0.13	0.13	0.16
Mulliken charge (e)	As(1)	1.28	1.27	0.81
	As(2)	1.29	1.27	1.17
	O(1)	-1.03	-1.02	-1.03
	O(2)	-1.02	-1.01	-1.04
	O(3)	-0.88	-0.87	-0.90
	O(4)	-1.04	-1.03	-1.04
	Al(1)	1.74	1.73	1.77
	Al(2)	1.82	1.79	1.87
	Ca(1)	1.36	1.29	1.29

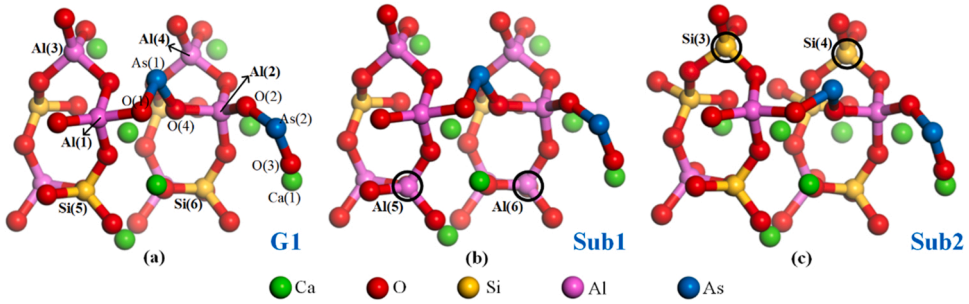

Fig. 11. Structures of adsorption before and after rearrangement of Si/Al: (a) G1 (before rearrangement); (b) Sub1; (c) Sub2.

minerals [20]. Modifying Ca-based mineral adsorbents with Si and Al can also enhance their adsorption ability in future studies [52].

CRediT authorship contribution statement

Guo–chang Song: Conceptualization, Methodology, Formal analysis, Investigation, Writing – original draft. **Xing–yu Yang:** Methodology, Validation, Writing **–** review & editing, Resources, Visualization. **Zhong-wei Li:** Methodology, Validation, Writing – review & editing. **Qiang Song:** Writing – review & editing, Supervision, Project administration, Funding acquisition.

Declaration of Competing Interest

The authors declare that they have no known competing financial interests or personal relationships that could have appeared to influence the work reported in this paper.

Data availability

Data will be made available on request.

Acknowledgements

This work was financially supported by the China National Key Research and Development Program (2022YFC3701503) and the Fundamental Research Funds for the Central Universities of China (2022ZFJH004).

Appendix A. Supporting information

Supplementary data associated with this article can be found in the online version at doi:10.1016/j.jece.2023.110271.

References

[1] L.B. Clarke, L.L. Sloss, Trace elements - emissions from coal combustion and gasification, IEA Coal Res. 49 (1992) 36–37.
[2] Z. Rahman, V.P. Singh, The relative impact of toxic heavy metals (THMs) (arsenic (As), cadmium (Cd), chromium (Cr)(VI), mercury (Hg), and lead (Pb)) on the total environment: an overview, Environ. Monit. Assess. 191 (2019) 419.
[3] R.B. Finkelman, Potential health impacts of burning coal beds and waste banks, Int. J. Coal Geol. 59 (2004) 19–24.
[4] N. Rodella, A. Bosio, A. Zacco, L. Borgese, M. Pasquali, R. Dalipi, L.E. Depero, V. Patel, P.A. Bingham, E. Bontempi, J. Environ. Chem. Eng. 2 (2014) 1352–1357.
[5] H.Z. Tian, C.Y. Zhu, J.J. Gao, K. Cheng, J.M. Hao, K. Wang, S.B. Hua, Y. Wang, J. R. Zhou, Quantitative assessment of atmospheric emissions of toxic heavy metals from anthropogenic sources in China: historical trend, spatial distribution, uncertainties, and control policies, Atmos. Chem. Phys. 15 (2015) 10127–10147.
[6] U.S. Environmental Protection Agency, National Emission Standards for Hazardous Air Pollutants from coal and oil–fired electric utility steam generating units and standards of performance for fossil–fuel–fired electric utility, industrial–commercial–institutional, and small industrial–commercial–institutional steam generating units, Fed. Regist. 77 (32) (2012) 9487–9488.
[7] European Union. Directive (EU) 2016/2284 of the European Parliament and of the Council of 14 December 2016 on the reduction of national emissions of certain atmospheric pollutants, amending Directive 2003/35/EC and repealing Directive 2001/81/EC. Official Journal of the European Union 2016; 344, 1–31.
[8] S.L. Zhao, Y.F. Duan, L. Chen, Y.N. Li, T. Yao, S. Liu, M. Liu, J.H. Lu, Study on emission of hazardous trace elements in a 350 MW coal–fired power plant. Part 2. arsenic, chromium, barium, manganese, lead, Environ. Pollut. 226 (2017) 404–411.
[9] J.W. Wang, Y.S. Zhang, Z. Liu, Y.Z. Gu, P. Norris, H. Xu, W.P. Pan, Coeffect of air pollution control devices on trace element emissions in an ultralow emission coal–fired power plant, Energy Fuels 33 (2019) 248–256.
[10] T. Czech, A. Marchewicz, A.T. Sobczyk, A. Krupa, A. Jaworek, Ł. Śliwiński, D. Rosiak, Heavy metals partitioning in fly ashes between various stages of electrostatic precipitator after combustion of different types of coal, Process Saf. Environ. Prot. 133 (2020) 18–31.
[11] W.S. Seames, J.O.L. Wendt, Partitioning of arsenic, selenium, and cadmium during the combustion of Pittsburgh and Illinois #6 coals in a self–sustained combustor, Fuel Process. Technol. 63 (2000) 179–196.
[12] P. Ji, G.C. Song, W.T. Xu, Q. Song, Transformation characteristics of arsenic and lead during coal combustion, Energy Fuels 33 (2019) 9280–9288.
[13] L.M. Zhou, H. Guo, X.B. Wang, M. Chu, G.J. Zhang, L.G. Zhang, Effect of occurrence mode of heavy metal elements in a low rank coal on volatility during pyrolysis, Int. J. Coal Sci. Technol. 6 (2019) 235–246.
[14] G.C. Song, W.T. Xu, X.Y. Yang, Q. Song, Retention of As during coal combustion: devolatilization and char combustion, Process Saf. Environ. Prot. 167 (2022) 203–212.
[15] G.C. Song, W.T. Xu, X.Y. Yang, Q. Song, Coupling effects of mineral components on arsenic transformation during coal combustion, J. Hazard. Mater. 435 (2022), 129040.
[16] J.W. Wang, Y.S. Zhang, T. Wang, H. Xu, W.P. Pan, Effect of modified fly ash injection on As, Se, and Pb emissions in coal–fired power plant, Chem. Eng. J. 380 (2020), 122561.
[17] W.T. Xu, G.C. Song, K.X. Hu, Q. Song, Q. Yao, The redistribution of arsenic during the interaction between high-temperature flue gas and ash, Fuel Process. Technol. 212 (2021), 106641.
[18] W.T. Xu, G.C. Song, X.Y. Yang, Q. Song, Q. Yao, Study on the chemical adsorption of gaseous As_2O_3 by ash, Fuel 330 (2022), 125557.
[19] P.B. Hu, S.J. Wang, Y.Q. Zhuo, Research on As_2O_3 adsorption enhancement characteristics of Mn-modified γ-Al_2O_3, Chem. Eng. J. 426 (2021), 131660.
[20] R.D. Zhao, R.W. Dai, T.J. Chen, J.G. Qin, J.Z. Zhang, J.H. Wu, Investigation on combustion, gaseous pollutants emission and ash characteristics during co-combustion of semicoke and coal slime, J. Environ. Chem. Eng. 9 (2021), 106249.
[21] W. Jerzak, P. Murzyn, M. Kuźnia, A. Magiera, Trace elements retention in bottom ashes during coal combustion with hydrated lime additions, Energy Sources Part A 43 (2021) 1215–1226.
[22] K.Q. He, C.G. Yuan, M.D. Shi, Y.H. Jiang, Accelerated screening of arsenic and selenium fractions and bioavailability in fly ash by microwave assistance, Ecotoxicol. Environ. Saf. 187 (2020), 109820.
[23] J.K. Han, D.X. Yu, Q.Y. Wang, N. Yu, J.Q. Wu, Y. Liu, L. Luo, H.X. Pan, Beneficiation of coal ash from ash silos of six Chinese power plants and its risk assessment of hazardous elements for land application, Process Saf. Environ. Prot. 160 (2022) 641–649.
[24] W.S. Seames, J.O.L. Wendt, Regimes of association of arsenic and selenium during pulverized coal combustion, Proc. Combust. Inst. 31 (2007) 2839–2846.
[25] H.Y. Gong, Y.D. Huang, H.Y. Hu, B. Fu, T.T. Ma, S. Li, et al., Insight of particulate arsenic removal from coal-fired power plants, Fuel 257 (2019), 116018.
[26] Y. Yu, R.H. Zhao, X.Y. Li, J. Chen, Y. Dong, Mechanism of CaO and Fe_2O_3 capture gaseous arsenic species in the flue gas: DFT combined thermodynamic study, Fuel 312 (2022), 122838.
[27] S.H. Yu, C. Zhang, L. Ma, Q.Y. Fang, G. Chen, Insight into As_2O_3 adsorption characteristics by mineral oxide sorbents: experimental and DFT study, Chem. Eng. J. 420 (2021), 127593.
[28] Y. Cao, B. Song, M. Song, F.Y. Meng, Y.X. Wei, Q. Cao, Capture of arsenic in coal combustion flue gas at high temperature in the presence of $CaSiO_3$ with good anti-sintering, Fuel Process. Technol. 205 (2020), 106428.
[29] Z.L. He, B. Song, C. Liang, B. Liu, Z.R. Ma, K.L. Pang, J.G. Yang, Insight into high temperature gas-phase arsenic capture by a $CaO-Ca_{12}Al_{14}O_{33}$ synthetic sorbent, Energy Fuels 35 (2021) 2425–2433.
[30] B. Song, M. Song, D.D. Chen, Y. Cao, F.Y. Meng, Y.X. Wei, Retention of arsenic in coal combustion flue gas at high temperature in the presence of CaO, Fuel 259 (2020), 116249.
[31] D.K. Chen, H.Y. Hu, Z. Xu, H. Liu, J.X. Cao, J.H. Shen, H. Yao, Findings of proper temperatures for arsenic capture by CaO in the simulated flue gas with and without SO_2, Chem. Eng. J. 267 (2015) 201–206.
[32] C. Wen, X.P. Gao, M.H. Xu, A CCSEM study on the transformation of included and excluded minerals during coal devolatilization and char combustion, Fuel 172 (2016) 96–104.
[33] J.R. Zha, Y.J. Huang, W.Q. Xia, Z.P. Xia, C.Q. Liu, L. Dong, L.Q. Liu, Effect of mineral reaction between calcium and aluminosilicate on heavy metal behavior during sludge incineration, Fuel 229 (2018) 241–247.
[34] G.C. Song, W.T. Xu, K. Liu, Q. Song, Transformation of selenium during coal thermal conversion: effects of atmosphere and inorganic content, Fuel. Process. Technol. 205 (2020), 106446.
[35] Y.M. Fan, Q.Y. Weng, Y.Q. Zhuo, S.T. Dong, P.B. Hu, D.L. Li, Theoretical study of As_2O_3 adsorption mechanisms on CaO surface, Materials 12 (2019) 677.
[36] X.Y. Li, J. Chen, R.H. Zhao, Z.P. Xiong, C.M. Lu, Determination on the activity of formed $CaSO_4$ for arsenic adsorption during arsenic capture by CaO with the presence of SO_2: experimental and density functional theory study, Chem. Eng. J. 427 (2022), 132015.
[37] H.X. Xing, H. Liu, X.J. Zhang, Y.D. Huang, H.Y. Li, B. Huang, H.Y. Hu, H. Yao, In-furnace control of arsenic vapor emissions using kaolinite during low-rank coal combustion: influence of gaseous sodium compounds, Environ. Sci. Technol. 53 (2019) 12113–12120.
[38] J.D. Hong, Y.F. Zhao, J. Wu, X.L. Xie, P.C. Zhao, S. Li, H. Yao, G.Q. Luo, Z.H. Liu, X. Yang, Fabrication of Al_2O_3/CaO with anti-sintering for efficient removal of As_2O_3 in simulated flue gas: experimental and DFT study, Fuel 307 (2022), 121812.
[39] S. Li, Z.P. Zhang, Q.Y. Liu, J.D. Hong, Y. Ling, M.L. Zhang, Q.Z. Liu, J. Wu, G. Q. Luo, H. Yao, X.L. Xie, P.C. Zhao, Preparation of CeO_2/CaO with anti-sintering for efficient capture of As_2O_3 from flue gas at a high temperature, Energy Fuels 35 (2021) 20197–20205.
[40] G.C. Song, W.T. Xu, P. Ji, Q. Song, Study on the transformation of arsenic and lead in pyrite during thermal conversion, Energy Fuels 33 (2019) 8463–8470.
[41] S.J. Clark, M.D. Segall, C.J. Pickard, P.J. Hasnip, M.I. Probert, K. Refson, M. C. Payne, First principles methods using CASTEP, Cryst. Mater. 220 (2005) 567–570.

[42] K. Burke, M. Ernzerhof, J.P. Perdew, Generalized gradient approximation made simple, Phys. Rev. Lett. 77 (1996) 3865–3868.
[43] D. Vanderbilt, Soft self-consistent pseudopotentials in a generalized eigenvalue formalism, Phys. Rev. B Condens. Matter 41 (1990) 7892–7895.
[44] W.H. Press, S.A. Teukolsky, W.T. Vetterling, B.P. Flannery. Numerical Recipes in C, second ed., Cambridge University Press, Cambridge, UK, 1996.
[45] I.P. Swainson, M.T. Dove, W.W. Schmahl, A. Putnis, Neutron diffraction study of the akermanite-gehlenite solid solution series, Phys. Chem. Miner. 19 (1992) 185–195.
[46] S. Thayaparam, M.T. Dove, V. Heine, A computer simulation study of Al/Si ordering in gehlenite and the paradox of the low transition temperature, Phys. Chem. Miner. 21 (1994) 110–116.
[47] F. Zhang, X.Q. Liu, X. He, H.M. Zhao, W. Chu, Y. Xue, A periodic density functional theory study of adsorption of CO_2 on anorthite (001) surface and effect of water, J. Theor. Comput. Chem. 18 (2019) 1950010.
[48] Y. Ling, J.C. Li, C. Zou, J. Wu, P.C. Zhao, X.L. Xie, Y.F. Qi, Q.Z. Liu, J.D. Hong, S. Li, Interaction mechanism between gaseous arsenic and the unburned carbon in coal-fired fly ash: a DFT combined thermodynamics study, Chem. Eng. J. 425 (2021), 130714.
[49] P. Florian, E. Veron, T.F.G. Green, J.R. Yates, D. Massiot, Elucidation of the Al/Si ordering in gehlenite $Ca_2Al_2SiO_7$ by combined ^{29}Si and ^{27}Al NMR spectroscopy/quantum chemical calculations, Chem. Mater. 24 (2012) 4068–4079.
[50] K. Mohammad, A review on the adsorption of heavy metals by clay minerals, with special focus on the past decade, Chem. Eng. J. 308 (2017) 438–462.
[51] J.B. Awuah, N.Y. Dzade, R. Tia, E. Adei, B. Kwakye-Awuah, C.R.A. Catlow, N. H. Leeuw, A density functional theory study of arsenic immobilization by the Al (iii)- modified zeolite clinoptilolite, Phys. Chem. Chem. Phys. 18 (2016) 11297–11305.
[52] L. Zhao, K. Shen, B.B. Li, Y.P. Zhang, S.L. Zhang, Y.M. Hong, J.P. Zhang, Z.Y. Li, Exploration of novel high-temperature heavy metals adsorbent for sludge incineration process: experiments and theoretical calculations, J. Environ. Chem. Eng. 10 (2022), 107755.